Proximity Loss Considerations for Compact Multiturn Transmitting Loop Antennas at HF

W. Perry Wheless, Jr., Swati Maheshwari, and Michael A. McNees
Department of Electrical and Computer Engineering
The University of Alabama
Tuscaloosa, AL 35487
Contact Email: wwheless@eng.ua.edu

***Abstract*— Progress in a continuing research project is reported here. The objective of the research is to quantify the feasibility of using physically compact RF inductors as effective transmitting antennas for HF (3-30 MHz) communications. Proximity losses for the closely spaced turns of helically wound, air core RF inductors fabricated with either wire or tubing are substantial, and must be accounted for in any predictive model. A capability for estimation of total loss (proximity loss plus high-frequency ac ohmic loss) has been developed which, when combined with radiation pattern and gain calculations from a numerical method such as the Method of Moments (MoM), gives a more accurate and reliable prediction of performance for a coil antenna than is available from MoM or proximity loss values, taken individually.**

I. Introduction

There is considerable interest in small antennas for HF radio communication applications, especially in the context of portable and mobile operations. The geometry under consideration here is helically wound, air core RF inductors, fabricated with wire or tubing. A specific example is the coil (RF inductor) whose photograph appears in Figure 1. This 57 μH inductor is made with 1.27 cm (0.5 inch) diameter silver-plated copper tubing. There are 22 turns, total, in a length of 44 cm (slightly more than 17 inches), so the center-to-center turn spacing is 2 cm. The coil diameter is approximately 30 cm (12 inches). This particular RF inductor was originally part of an antenna tuning unit (ATU) circuit at a 50 kW AM broadcast station.

The coil axis in Figure 1 is vertically aligned, with a section of 10 cm (4 inch) diameter PVC pipe supporting the frame of the coil and providing a nominal elevation of approximately 0.6m above the large plywood dolly base which is partially visible in the lower part of the photograph. Two of three bars for securing the coil turns in place are clearly visible in Figure 1, and these support structures are made of micalex. To create a feed point, a gap of approximately 1.25 cm was created by cutting that length out of the coil tubing and soldering two heavy brass tabs with 0.25-inch brass hardware to secure the center conductor and braid, respectively, of RG-8 50Ω coaxial cable. A short section of coax is shown attached to the coil in Figure 1; note the black heatshrink (toward the lower left in the picture) which secures six cylindrical ferrite chokes to the cable.

Figure 1. A compact coil (multi-turn loop) antenna.

II. Background

An early source of interest in loop antenna configurations for HF communications was the quad antenna, generally credited to Clarence Moore as his solution to corona discharge problems with yagis at high altitude while he was at the shortwave missionary radio station HCJB in Quito, Ecuador, in the early 1940s. A basic two-element quad array is depicted in Figure 2. The driven elements are electrically 1λ in circumference (i.e., $\frac{\lambda}{4}$ on each side), and the reflectors are slightly longer.

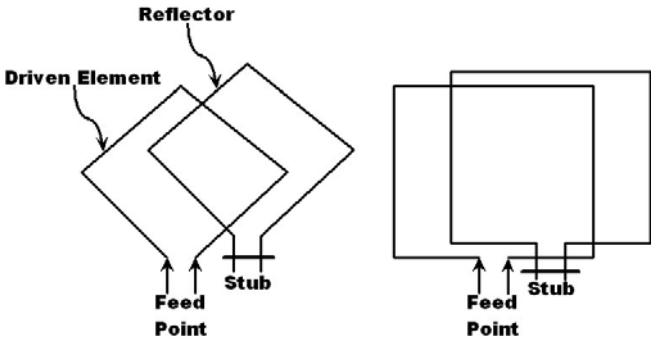

Figure 2. Basic two-element quad array.

Quad-yagi comparisons suggests that the quad excels with respect to gain, is similar in SWR characteristics, and lags with respect to front-to-back ratio. Favorable experience in applications solidified the quad as a popular directional wire antenna for both the HF and VHF spectrum. The principal drawback of the full-sized quad is that it is physically cumbersome to construct and deploy. Physical size of the quad may fairly be described as large at frequencies below 14 MHz, becoming preclusive below 7 MHz.

As a compromise, the amateur radio community led the quick adaptation to using the driven element from a quad array alone as a single loop. Experiments with the loop mounted horizontally soon followed and this work, in turn, inspired efforts toward emulating 1λ loop performance with versions of reduced size. One of the more complete collection of practical guidelines to HF compact loop construction is in [1], which contains specific designs [2] as well.

The next logical step in compact loop antenna development was multiturn loops, and this class of physically small antennas has received some attention over the past thirty years (see, for example, [3]). Clever variations on the simple circular or square loop geometries have been devised, such as the incorporation of fractals [4], [5]. Nonetheless, more success has been achieved with small multiturn loop receiving antennas [6] than with transmitting antennas.

III. Terminology

Loops are generally divided into two classes: those loops for which the total conductor length and maximum linear dimension of a turn are very small relative to the operating wavelength, and those for which the total conductor length and loop dimensions become comparable to the wavelength.

A more precise definition of an electrically small loop is one in which the current has the same magnitude and phase everywhere in the loop. To reasonably comply with this condition, the working compromise is that the loop's total conductor length should not exceed (approximately) 0.1λ. A "large" loop, then, is one in which the current amplitude and phase are not required to be constant everywhere in the loop. In practice, a conductor length of 0.5λ is generally taken to be the minimum for a loop to be described as large.

Especially for portable and/or mobile operation, physical size is the more important parameter. Therefore, the descriptor "compact" has been adopted here to identify the class of (potential) multiturn loop antennas of interest, and is hereafter the shorthand notation for "physically compact." In some cases, a physically compact multiturn loop (that is, a coil) may qualify as electrically small at certain proposed frequencies of operation, and simultaneously qualify as electrically large at other higher operating frequencies.

IV. Efficiency and Proximity Loss

A straightforward measure of antenna radiation efficiency is given by

$$\eta = \frac{R_{Rad}}{R_{Rad} + R_{Loss}}, \tag{1}$$

usually expressed as a percentage.

For a single-turn transmitting loop, R_{Loss} is essentially the conductor's ac resistance (but also includes connection resistances and embedded tuning reactance losses which are generally negligible when $R_{Rad} > 0.25\Omega$), approximated by

$$R_{ac} = \frac{0.996 \times 10^{-6}\sqrt{f}}{d} \tag{2}$$

with frequency f in Hz, conductor diameter d expressed in inches, and R_{ac} in Ohms per foot. Skin effect is responsible for increasing the effective resistance as frequency is increased, corresponding to the increased energy loss experienced by fluids forced to maintain a constant flow rate when directed into a pipe of smaller diameter. Anecdotal accounts of practical experience suggests that the loop conductor should be at least 0.75 inch diameter, if made of copper, to achieve reasonable transmit efficiency.

For multiturn loops with turns closely spaced, there is an additional loss arising from what is known as *proximity effect*. The source of the observed effect is the fact that the circumferential current distribution changes as the current-carrying coil turns are brought close together, changing the surface current (per square meter) flowing at surfaces adjacent to other conductors. Higher loss than suggested by a skin effect analysis results because the current flow is compressed and flows through a smaller cross-sectional area than if the neighboring turns were absent.

The order of magnitude of the effect is indicated in the following excerpt from page 5-12 of reference [1]:

> *As the efficiency of a loop antenna approaches 90%, the proximity effect is less serious. But unfortunately, the less efficient the loop, the worse the effect. For example, an 8-turn transmitting loop with an efficiency of 10% (calculated by the skin-effect method) actually only has an efficiency of 3% because of the additional losses introduced by the proximity effect.*

When the coil conductor is segmented for Moment Method analysis by a code such as EZNEC, the numerical procedure returns a complex (magnitude/phase) current value for each

segment. However, it appears that closely spaced parallel conductors pose a challenge for the numerical technique, and that it does not account for the significant current compression loss associated with the proximity effect. The plausibility of this conclusion has been investigated by means of the following specific case study.

V. A Specific Case Study: Gates ATU Coil

The RF inductor shown in the photograph of Figure 1 was selected for a detailed engineering study. This 57 μH coil was originally manufactured by Gates Radio Company for use in high-power AM broadcast service. Its relatively large diameter silver-plated tubing and turn-to-turn spacing that was originally selected for MF applications suggested that this coil might hold significant promise for use as a transmitting antenna at HF.

To begin, the coil geometry was segmented (using an octagonal approximation to its circular cross section), similar to the illustration in Figure 3, and preliminary numerical analysis conducted with the Method of Moments code EZNEC [16]. For purposes of this study, the following specific frequencies were selected: 1.9, 3.8, 7.3, 10.1, 14.25, 18.1, and 21.3 MHz. These frequencies are all in, or at the edge of, amateur radio bands so that transmit as well as receive experiments could be conducted. Figures 4 and 5 illustrate the elevation pattern results obtained.

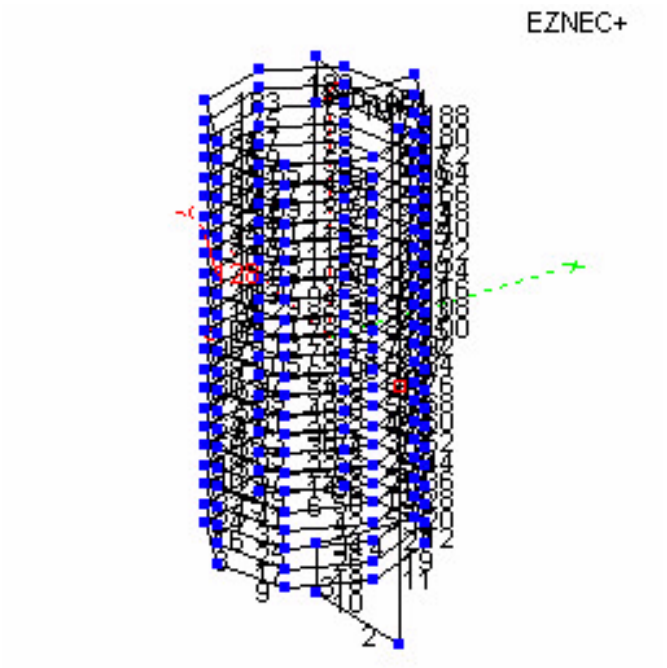

Figure 3. MoM segmentation, octagonal approximation.

Because the total conductor length of the coil tubing is about 22 m, approaching half-wavelength natural resonance length near the 7 MHz (40 meter) band, and armed with the -4.51 dBi gain prediction for 7.3 MHz from the computer analysis, it was decided to initiate experimental observations in the 40m band. The coil center-feed terminals were connected to the output of a MFJ HF antenna tuning unit, as shown in the photograph of Figure 6 through a section of 50Ω that was less than 1 meter in length. From there, another 15-meter long 50Ω coaxial cable was used to connect the MFJ tuner input to a 100W HF transceiver inside.

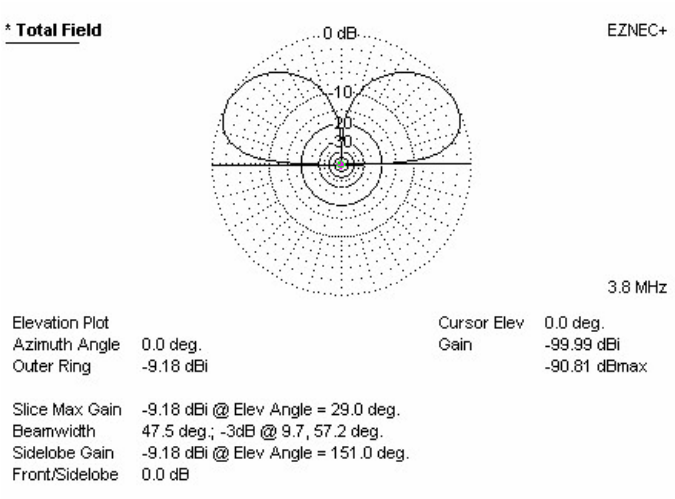

Figure 4. Elevation plot for 3.8 MHz.

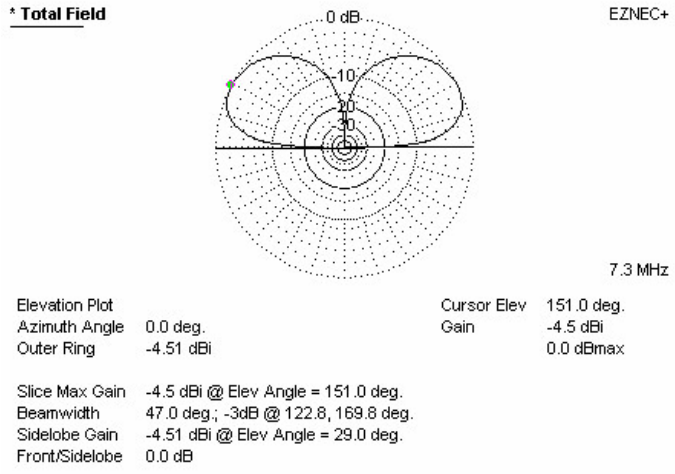

Figure 5. Elevation plot for 7.3 MHz.

Numerous radio contacts were made in the 40m amateur bands with the coil deployed on its plywood dolly inside the bed of a pickup truck (see photograph in Figure 6, which shows the coil antenna being connected to the ATU), and the immediate results were exhiliarating. Both transmit and receive signals were fully comparable to a full sized horizontal center-fed dipole mounted at approximately 40 feet (12.2 m). In some instances, the coil exhibited superior

performance! Since the 21 MHz (15m) amateur band is at an odd multiple of 40m, so the coil conductor length again approaches a natural resonance, contacts on the 15m band followed - with similarly astonishing results. From Alabama, first-day contacts included stations from Africa to Asia.

Figure 6. Coil on platform in truck bed.

Unfortunately, when cylindrical coax-diameter ferrite "beads" were placed on the cable section between the coil feed point and the ATU, the performance on both 40m and 15m plummeted. All those bodacious signals and superlative long-distance signal reports were mostly attributable to currents flowing on the outside of the coax braid and blind chance selection of a day with outstanding propagation conditions for the initial testing!

Six ferrite chokes were added to the short coil feed pigtail, secured by enclosure with heatshrink tubing, and the "choked" pigtail connector was used in all subsequent experimentation.

Seeking an explanation for the large discrepancy subsequently observed between NEC2 performance prediction and actual practice, the compact coil HF antenna project proceeded to obtain quantitative results for potentially significant additional proximity effect losses.

VI. Proximity Loss Program Introduction

A literature search revealed that Glenn Smith, now a professor of electrical engineering at Georgia Tech, conducted the most thorough scientific study available of proximity loss. Dr. Smith's work dates from the early 1970s, while he was still working with R.W.P. King at Harvard University. It was deemed a necessity to be able to reproduce the results reported in his papers, principally [7], and to develop a modernized computer code (in MATLAB [8]) which would allow contemporary users to make proximity loss predictions about coils of geometries (and operating frequencies) different from those of high priority to Dr. Smith in his original work.

VII. Mathematical Preliminaries

In [7], the solutions for two cases of proximity loss calculation are treated. First, in the case when two parallel, closely-spaced cylindrical conductors are present, the Jacobi elliptic integrals and functions are used to determine the normalized current distribution in each conductor and, also, the normalized additional ohmic resistance per unit length due to the proximity effect. In the second case, that of an even number of conductors (greater than two), a least squares methodology is used. The second case will be addressed later; some review remarks about the elliptic integrals and functions relevant to the first case are made here.

Jacob Bernoulli encountered a form of elliptic integral in 1679 and, in 1694, he made an important step in the theory of elliptic integrals. See [9] for a brief tutorial on the elliptic integral, from which the following excerpt is taken:

> *Elliptic integrals can be viewed as generalizations of the inverse trigonometric functions and provide solutions to a wider class of problems. For instance, while the arc length of a circle is given as a simple function of the parameter, computing the arc length of an ellipse requires an elliptic integral. Similarly, the position of a pendulum is given by a trigonometric function as a function of time for small angle oscillations, but the full solution for arbitrarily large displacements requires the use of elliptic integrals. Many other problems in electromagnetism and gravitation are solved by elliptic integrals.*
>
> *A very useful class of functions known as elliptic functions is obtained by inverting elliptic integrals to obtain generalizations of the trigonometric functions. Elliptic functions (among which the Jacobi elliptic functions and Weierstrass elliptic function are the two most common forms) provide a powerful tool for analyzing many deep problems in number theory, as well as other areas of mathematics.*

Theorem 1: If $R(x,y)$ is a rational function in x and $y = \sqrt{P(x)}$, namely

$$R(x,y) = \int \frac{A(x)dx}{B(x)} \overset{OR}{=} \int \frac{A(x)+B(x)\sqrt{P(x)}}{C(x)+D(x)\sqrt{P(x)}}dx \quad (3)$$

where $P(x)$ is a polynomial of degree three or four with no repeated factors, then the integral

$$\int R(x,\sqrt{P(x)})dx \equiv \int R(x,y)dx \quad (4)$$

can always be expressed in terms of elliptic integrals [13]. For a proof, see [14].

It is necessary to apply the above theorem to achieve an analytical solution for the proximity loss associated with a pair of conductors, and there are three classifications of elliptic integrals:

$$\underline{1^{st} \text{ Kind:}}\ F(k,\phi) = \int_0^{\phi} \frac{d\theta}{\sqrt{1-k^2\sin^2\theta}}, \quad 0<k<1 \quad (5)$$

$$\underline{2^{nd}\text{:}}\ E(k,\phi) = \int_0^{\phi} \sqrt{1-k^2\sin^2\theta}\, d\theta, \quad 0<k<1 \tag{6}$$

$$\underline{3^{rd}\text{:}}\ \Pi(k,\phi,a) = \int_0^{\phi} \frac{d\theta}{\sqrt{1-k^2\sin^2\theta}\left(1+a^2\sin^2\theta\right)}, \tag{7}$$

$$\text{for } \begin{cases} 0<k<1 \\ a\neq k,0 \\ n=-a^2 \end{cases}.$$

Parameter ϕ is called the *amplitude* and k the *modulus*. Number n is called the characteristic and can take any value $(-\infty,\infty)$ regardless of other variables. When $\phi=\frac{\pi}{2}$, these become known as the *complete elliptic integrals*, with the special designations

$$\begin{aligned} &\underline{1^{st}\text{ Kind:}} && F(k,\tfrac{\pi}{2}) \Longrightarrow K(k)=K \\ &\underline{2^{nd}\text{ Kind:}} && E(k,\tfrac{\pi}{2}) \Longrightarrow E(k)=E \\ &\underline{3^{rd}\text{ Kind:}} && \Pi(k,\tfrac{\pi}{2},a) \Longrightarrow \Pi(k,a)=\Pi. \end{aligned} \tag{8}$$

Useful infinite series representations for K and E, and results for limiting cases $m\to 0$ and $m\to 1$ are well known and readily available in references such as [13], [15]. Inversion of elliptic integrals leads to elliptic functions which fall into two categories - the Weierstrass and Jacobi elliptic functions, with the Jacobi elliptic functions considered the standard form. The three basic Jacobi functions are

$$\begin{aligned} sn(u) &= sn\ u = \sin\phi = x \\ cn(u) &= cn\ u = \cos\phi \\ dn(u) &= dn\ u = \sqrt{1-m\sin^2\phi} \end{aligned} \tag{9}$$

with the third relation giving $\phi=\arcsin(sn\ u)$ =am u, the amplitude. The Jacobian elliptic functions are doubly periodic. K and iK' are the "real" and "imaginary" quarter-periods of these functions, defined by

$$K(m) = K = \int_0^{\frac{\pi}{2}} \frac{d\theta}{\sqrt{1-m\sin^2\theta}} \tag{10}$$

and

$$iK'(m) = iK' = i\int_0^{\frac{\pi}{2}} \frac{d\theta}{\sqrt{1-m'\sin^2\theta}} \tag{11}$$

with $0<m<1$ and $m+m'=1$. Both K and K' are real numbers. Finally, if one wishes to use the modulus k instead of the parameter m, equations 10 and 11 become

$$K(k) = K = \int_0^{\frac{\pi}{2}} \frac{d\theta}{\sqrt{1-k^2\sin^2\theta}} \tag{12}$$

and

$$iK'(k) = iK' = i\int_0^{\frac{\pi}{2}} \frac{d\theta}{\sqrt{1-(k')^2\sin^2\theta}} \tag{13}$$

where $(k')^2 = 1-k^2$.

TABLE I

Elliptic Integral Reference Table of Variables

Variable	**Description**
k	Modulus
k'	Complementary Modulus
$m=k^2=\sin^2\alpha$	Parameter
$m'=1-m$	Complementary Parameter
$\alpha=\sin^{-1}k$	Modular Angle
$\phi=$ am u	Amplitude
$q=e^{-\frac{iK'}{K}}$	Nome
$K=K(k)$	Quarter Period
$K'=K(k')$	Imaginary Quarter Period

VIII. Solution for Two Wires

For the two cylindrical wires case, assuming constant (i.e., equal) current flowing in both conductors, the analytical solution in [7] uses Jacobi elliptic integrals and functions to calculate the normalized current distribution on each conductor and, from that, the normalized additional ohmic resistance per unit length arising from the proximity effect. Smith [7] adapted the conformal mapping electrostatic solution reported by Whipple [10] to the context of the problem of present interest, and arrived at the following as the solution for the normalized current distribution (Eq. 30 in [7]):

$$\begin{aligned} g(\theta) \;=\; & \frac{2(1+k)K(k)}{\pi}\ \text{csch}\ \alpha(\cosh\alpha-\cos u) \\ & \times dn\left(\frac{(1+k)K(k)}{\pi}u, \frac{2\sqrt{k}}{1+k}\right) \end{aligned} \tag{14}$$

with

$$u = \sin^{-1}\left(\frac{\sin\theta \sinh\alpha}{c/a + \cos\theta}\right)$$

$$\alpha = \ln\left[\frac{a}{c - (c^2 - a^2)^{\frac{1}{2}}}\right]$$

$$\frac{K'(k)}{K(k)} = \frac{2\alpha}{\pi} \tag{15}$$

$$0 \le u \le \frac{\pi}{2} \text{ for } 0 \le \theta \le \cos^{-1}\left(\frac{a}{c}\right)$$

$$\frac{\pi}{2} \le u \le \pi \text{ for } \cos^{-1}\left(\frac{a}{c}\right) \le \theta \le \pi.$$

in addition to the entries of Table I. Calculation of the modulus k requires the so-called theta functions, summarized in Table II below.

Table II

Theta Functions

$\Theta_1(z,q) = \Theta_1(z) = 2q^{\frac{1}{4}} \sum_{n=0}^{\infty} (-1)^n q^{n(n+1)} \sin(2n+1)z$
$\Theta_2(z,q) = \Theta_2(z) = 2q^{\frac{1}{4}} \sum_{n=0}^{\infty} q^{n(n+1)} \cos(2n+1)z$
$\Theta_3(z,q) = \Theta_3(z) = 1 + 2\sum_{n=1}^{\infty} q^{n^2} \cos(2nz)$
$\Theta_4(z,q) = \Theta_4(z) = 1 + 2\sum_{n=1}^{\infty} (-1)^n q^{n^2} \cos(2nz)$

The normalized additional ohmic resistance per unit length attributable to proximity effect is then

$$\frac{R_p}{R_0} = \left(\frac{2K}{\pi}\right)^2 \left[2 \text{ ctnh } \alpha \left\{\frac{E(K,k)}{k} - \frac{(k')^2}{2}\right\}\right] - \left(1 + 2 \text{ csch}^2\alpha\right) \tag{16}$$

(Eq. 31 in [7]) where $E(K,k)$ is the complete elliptic integral of the second kind and $(k')^2 = 1 - k^2$).

Noting that $2c$ is the center-to-center conductor spacing and a is the conductor radius, the normalized surface current distributions as a function of angle θ (see Figure 7) for two conductors at various ratios $\frac{c}{a}$ are shown in Figure 8. The results, computed with MATLAB, closely emulate those in Fig. 3 of reference [7]. MATLAB does not have built-in support for all the elliptic functions, so custom code was written to calculate the elliptic function values for substitution into 16. The *half-period ratio* τ is related to the real and imaginary quarter periods by

$$\tau = \frac{iK'}{K} = \frac{2\alpha}{\pi}. \tag{17}$$

Subsequently, the value of *nome* is obtained from

$$q = e^{\frac{-\pi K'}{K}} = e^{i\pi\tau}. \tag{18}$$

Table II contains the theta function formulas used to calculate the elliptic modulus

$$k = \left(\frac{\Theta_2}{\Theta_3}\right)^2. \tag{19}$$

The value of z in the Table II relations is zero here. Parameter m is obtained from k, and is used as the argument in the MATLAB function "ellipj" to evaluate the elliptic integrals of the first and second kinds.

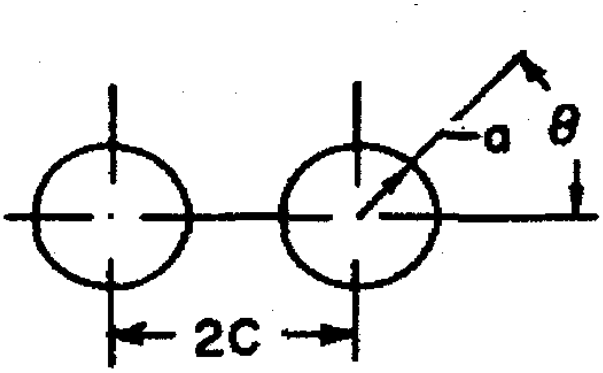

Figure 7. Two-conductor geometry.

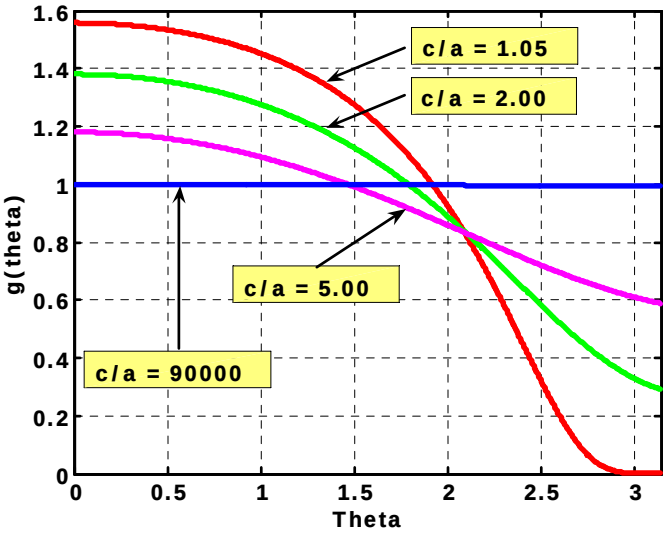

Figure 8. Normalized surface current distribution for different wire spacings.

IX. Solution for More Than Two Conductors

For more than two circular conductors, a closed form solution (in contrast to the two-wire case) cannot be found, and [7] proceeds to apply an approximation method - namely,

undetermined coefficients - to obtain current distributions and total ohmic resistance per unit length. Again, constant current is assumed. A trigonometric series is the expansion representation for the normalized surface current density:

$$g_m(\theta) = 1 + \sum_{p=1}^{q} a_{mp} \cos(p\theta) \tag{20}$$

where m is the wire number, q now represents the number of harmonics (and is not the nome, as before), and the a_{mp} factors represent Fourier coefficients. The simplification of an even number of wires in the system is taken. The Fourier coefficients are calculated via a matrix generated by the method of least squares, with an "Indicator function" involved in the process.

$$I(\theta, m-\ell, p) = \begin{cases} \dfrac{1}{(1-s^2)(-s)^{p+1}}(As^2 + Bs + C), \\ \qquad\qquad p = 1, 2, \ldots, q \\ \dfrac{-1}{s(1-s^2)}(Bs + 2C), \quad p = 0 \end{cases} \tag{21}$$

where

$$s = \left[4(m-\ell)^2 \left(\frac{c}{a}\right)^2 + 1 + 4(m-\ell)\left(\frac{c}{a}\right)\cos\theta\right]^{\frac{1}{2}}$$

$$A = \cos[\theta - (p-1)\Psi]$$

$$B = 2\left[1 + 2(m-\ell)\left(\frac{c}{a}\right)\cos\theta\right]\cos(p\Psi)$$

$$C = \cos[\theta + (p+1)\Psi]$$

$$\Psi = \pi - \tan^{-1}\left(\frac{\sin\theta}{2(m-\ell)\left(\frac{c}{a}\right) + \cos\theta}\right), \quad m - \ell = 1, 2, \ldots$$

$$\Psi = \tan^{-1}\left(\frac{-\sin\theta}{2(m-\ell)\left(\frac{c}{a}\right) + \cos\theta}\right), \quad m - \ell = -1, -2, \ldots$$

The equation key to determination of the coefficients a_{mp} can be written simplistically as

$$\sum_{p=1}^{q} a_{mp} t_{kp}^{m} + \sum_{\substack{\ell=1 \\ \ell \neq m}}^{\frac{n}{2}} \sum_{p=1}^{q} a_{mp} t_{kp}^{m\ell} = s_{mk}, \begin{cases} m = 1, 2, \ldots, \dfrac{n}{2} \\ k = 1, 2, \ldots, q \end{cases} \tag{22}$$

which is equivalent to the matrix equation

$$\begin{bmatrix} T_{11} & T_{12} & \cdots & T_{1,\frac{n}{2}} \\ T_{21} & T_{22} & \cdots & T_{2,\frac{n}{2}} \\ \vdots & \vdots & \ddots & \vdots \\ T_{\frac{n}{2},1} & T_{\frac{n}{2},2} & & T_{\frac{n}{2},\frac{n}{2}} \end{bmatrix} \begin{bmatrix} A_1 \\ A_2 \\ \vdots \\ A_{\frac{n}{2}} \end{bmatrix} = \begin{bmatrix} S_1 \\ S_2 \\ \vdots \\ S_{\frac{n}{2}} \end{bmatrix} \tag{23}$$

where the submatrices within the partitioned $\underset{\sim}{T}$ matrix are

$$T_{ii} = \begin{bmatrix} t_{11}^{i} & t_{12}^{i} & \cdots & t_{1,q}^{i} \\ t_{21}^{i} & t_{22}^{i} & \cdots & t_{2,q}^{i} \\ \vdots & \vdots & \ddots & \vdots \\ t_{q,1}^{i} & t_{q,2}^{i} & & t_{q,q}^{i} \end{bmatrix}, \; T_{ij} = \begin{bmatrix} t_{11}^{ij} & t_{12}^{ij} & \cdots & t_{1,q}^{ij} \\ t_{21}^{ij} & t_{22}^{ij} & \cdots & t_{2,q}^{ij} \\ \vdots & \vdots & \ddots & \vdots \\ t_{q,1}^{ij} & t_{q,2}^{ij} & & t_{q,q}^{ij} \end{bmatrix},$$

$$A_i = \begin{bmatrix} a_{i,1} \\ a_{i,2} \\ \vdots \\ a_{i,q} \end{bmatrix} \text{ and } S_i = \begin{bmatrix} s_{i,1} \\ s_{i,2} \\ \vdots \\ s_{i,q} \end{bmatrix}.$$

Expansion series coefficients a_{mp}, obtained by solving the matrix equation in standard fashion by multiplication with A^{-1}, are substituted into Eqn. (20) to give normalized surface current distribution graphs such as those in Figures 9 through 11 for the illustrative (half) spacing to radius ratio $\frac{c}{a} = 2$ in a 6-wire system. The results for conductors 4 (left middle) to 6 (left end) are known by symmetry. The interested reader should also see the original family of plots in Fig. 4 of reference [7], which are confirmed by the calculations done in this study.

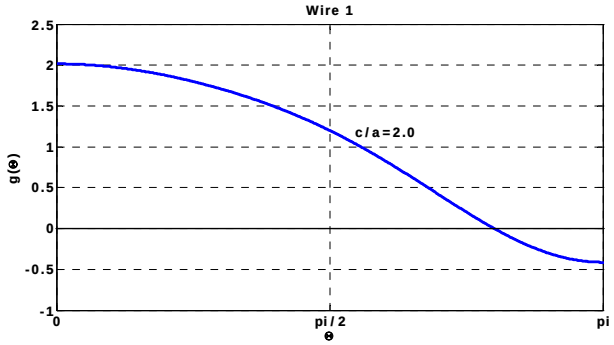

Figure 9. Surface current distribution, wire #1 (right end).

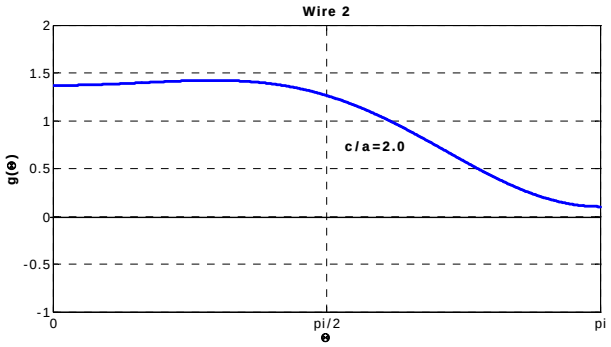

Figure 10. Surface current distribution, wire #2 (next to end).

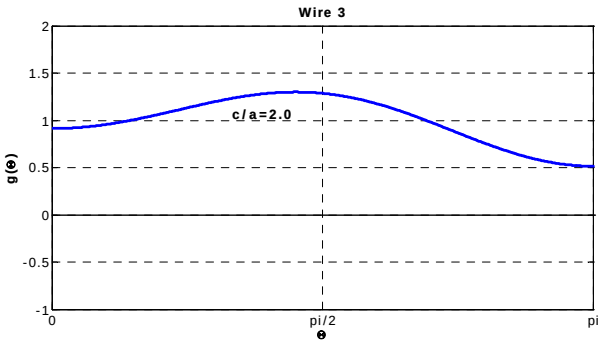

Figure 11. Surface current distribution, wire #3 (right middle).

The same a_{mp} coefficients are used to get the additional ohmic resistance per unit length due to proximity effect from

$$\frac{R_p}{R_0} = \frac{R - nR_R}{nR_R} = \frac{1}{2n}\sum_{m=1}^{n}\sum_{p=1}^{q}|a_{mp}|^2 \qquad \Omega/m \qquad (24)$$

where R_R is the Rayleigh formula for high-frequency resistance per unit length of a circular conductor, according to

$$R_R = \frac{2P}{|I|^2} = \frac{R^S}{2\pi a} = \frac{1}{2\pi a}\left(\frac{\omega\mu_0}{2\sigma}\right)^{\frac{1}{2}} \qquad \Omega/m \qquad (25)$$

$$\Longrightarrow R^S = \left(\frac{\omega\mu_0}{2\sigma}\right)^{\frac{1}{2}} \qquad (26)$$

and R is the ohmic resistance for n parallel wires, with all conductors carrying the same current, given by

$$R = \frac{R^S}{2\pi a}\sum_{m=1}^{n}\left(1 + \frac{1}{2}\sum_{p=1}^{q}|a_{mp}|^2\right). \qquad \Omega/m \qquad (27)$$

The right hand expression in Eqn. (24), with the double summation of $|a_{mp}|^2$, is the form used for practical calculations.

X. Specific Case Study

The subject specific case study is the multiturn loop (coil) transmitting antenna shown in Figure 1 and described in the "Introduction" section of this paper. For this 22-turn coil with $\frac{c}{a} = 1.667$ (center-to-center spacing of turns = 2 cm), after first calculating the $\underset{\sim}{T}$ and $\underset{\sim}{S}$ matrices discussed above, the matrix equation is solved for the coefficients ($\underset{\sim}{A}$ matrix) using MATLAB. Then the normalized additional resistance from the proximity effect follows from Eqn. (24):

$$\frac{R_p}{R_0} = \frac{1}{2n}\sum_{m=1}^{n}\sum_{p=1}^{q}|a_{mp}|^2 = 0.8979 \qquad \Omega/m \qquad (28)$$

Since the total conductor length for the coil is about 22 m,

$$\left(\frac{R_p}{R_0}\right)_{total\ prox} = 22 \times 0.8979 = 19.75\ \Omega \qquad (29)$$

and the total resistance per unit length (from 27) may be calculated from

$$R = \frac{\sqrt{\frac{2\pi f\mu_0}{2\sigma}}}{2\pi \times (0.6 \times 10^{-2})}\left[2 \times 22.16\right] = 0.30263\sqrt{f} \quad \frac{\Omega}{m}, \qquad (30)$$

noting that symmetry in the $|a_{mp}|^2$ numbers allows summation of half the index values to be computed $(= 22.16)$ and that result doubled $(\times 2)$.

For the subject coil antenna, selected numerical results are tabulated in Table III, where "Total R" is R in $\frac{\Omega}{m}$ multiplied by the conductor length 22.16 m, and loss in dB is from $10\log\left(\frac{Total\ R}{73}\right)$. The reference normalization value of $R_0 = 73\ \Omega$ was chosen because we wish to consider loss relative to the 73 Ω purely resistive input impedance associated with a naturally resonant half-wave dipole.

TABLE III

Case Study Resistance Results, $c/a = 1.667$

Freq. (MHz)	R (Ω/m)	Total R (Ω)	Loss in dB
1.9	417.1	9177.2	20.99
3.8	589.9	12978.5	22.50
7.3	817.7	17988.5	23.92
10.1	961.8	21158.8	24.62
14.25	1142.4	25132.8	25.37
18.1	1287.5	28325.11	25.89
21.3	1396.7	30727.2	26.24

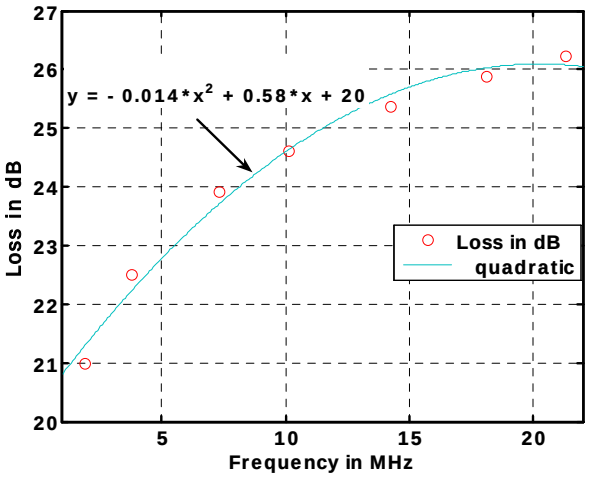

Figure 12. Proximity loss for Gates ATU coil.

As a brief but informative digression, Table IV hypothesizes about the results if the coil tubing radius a is held constant, but the turn-to-turn spacing is varied. The takeaway from Table IV is that, as expected, the proximity loss decreases as the turn spacing $2c$ is increased.

TABLE IV
Effect of Turn Spacing on Proximity Loss

Spacing $2c$ in cm	$\frac{c}{a}$	$\frac{R_p}{R_0}$ in $\frac{\Omega}{m}$
1.5	1.25	2.507
1.8	1.5	1.238
1.92	1.6	1.005
2.0	1.667	0.886
2.04	1.7	0.834
2.4	2.0	0.526
3.0	2.5	0.295
3.6	3.0	0.190
4.0	3.333	0.150
4.2	3.5	0.134
4.8	4.0	0.099

The plausibility of the "loss in dB" figures from Table III was tested experimentally, as discussed in the following section.

XI. Comparison to Measurements and Conclusions

The hypothesis is that NEC gain prediction by EZNEC and similar codes, even when real conductor loss is selected in the analysis program, is inadequate in the case of closely spaced parallel conductors such as in the case of the subject Gates ATU coil antenna. Further, it is asserted that the MoM numerical analysis fails to account for proximity loss, so that the addition of predicted proximity loss should give predicted gain values considerably closer to real-world signal observations.

A full measurements program has been only partially completed as of this writing. The results reported here, therefore, should be taken as significant but incomplete and reflective of conditions that do not allow the association of meaningful error bars. However, a preliminary interpretation may be made here with reasonable reliability.

The subject coil antenna was set up in an unobstructed area, with a 130-foot long horizontal dipole (at height approximately 13 m) in the near vicinity. Received signals at selected HF bands were observed by switching the two antennas, routed through MFJ tuners for impedance matching, into a Ten-Tec Corsair II receiver. Signal strength readings were taken from the analog front-panel S-meter of the Corsair II, which was determined to be calibrated to acceptable commercial radio standards. Incoming signals were from various (often unknown) compass bearings, distances (angles of arrival), and no attempt was made to correct for pattern effects of the large dipole at higher frequencies. Small data samples were collected on some seven different days. Propagation conditions made it difficult to acquire data at 18.1 MHz, and 21 MHz was essentially dead (any signals heard on the dipole were too weak to quantify accurately on the coil) on all days available for experimentation. The available data is presented in Table V below.

Table V

Predicted versus Measured Received Signal Strengths

(A) 3.8 MHz nominal	
Number of signal measurements:	**27**
Average measured coil vs dipole (dB):	**-38.3**
Proximity loss prediction:	**-22.5**
EZNEC gain (dBd) prediction:	**-11.4**
Sum of PL and EZNEC predictions:	**-33.9**
Discrepancy (measured-predicted) dB:	**-4.4**

(B) 7.2 MHz nominal	
Number of signal measurements:	**31**
Average measured coil vs dipole (dB):	**-20.6**
Proximity loss prediction:	**-23.9**
EZNEC gain (dBd) prediction:	**-6.7**
Sum of PL and EZNEC predictions:	**-30.6**
Discrepancy (measured-predicted) dB:	**+10.0**

(C) 10.1 MHz nominal	
Number of signal measurements:	**25**
Average measured coil vs dipole (dB):	**-20.5**
Proximity loss prediction:	**-24.6**
EZNEC gain (dBd) prediction:	**-5.25**
Sum of PL and EZNEC predictions:	**-29.85**
Discrepancy (measured-predicted) dB:	**+9.35**

(D) 14 MHz nominal	
Number of signal measurements:	**32**
Average measured coil vs dipole (dB):	**-28.3**
Proximity loss prediction:	**-25.4**
EZNEC gain (dBd) prediction:	**-4.3**
Sum of PL and EZNEC predictions:	**-29.7**
Discrepancy (measured-predicted) dB:	**+1.4**

(E) 18.1 MHz nominal	
Number of signal measurements:	**10**
Average measured coil vs dipole (dB):	**-29.4**
Proximity loss prediction:	**-25.9**
EZNEC gain (dBd) prediction:	**-3.9**
Sum of PL and EZNEC predictions:	**-29.8**
Discrepancy (measured-predicted) dB:	**+0.4**

The total conductor length for the subject coil gave a natural resonance close to the 7.0 - 7.3 MHz 40-meter band. This fact likely accounts for at least part of the unexpectedly good coil performance as an antenna in this nominal frequency range. It is also noteworthy that the 10.1 MHz (nominal) measurements included several instances, at different points in time, of measurements on the time standard station WWV in Fort Collins, Colorado. Similarly, the 7.2 MHz (nominal) measurements included several measurements, at different times, of the Canadian time standard CHU on 7.335 MHz.

Overall, the results presented in Table V clearly support the merit of the hypothesis that a correction for proximity loss should be added to pattern gain predictions from NEC in order to obtain electrical performance predictions more consistent with that generally observed in actual practice.

XII. Future Work and Final Remarks

It is apparent that more measured data is required to improve confidence in the preliminary conclusion reached here, especially in the vicinity of the 7.2 and 10.1 MHz bands. Additional measurements comparing coil and dipole received signal strengths will be made in the near future.

The calculation of proximity loss assumes constant current in all the coil turns. For the specific case study here, at 3.8 MHz a free space wavelength is close to 79 m, so the 22 m of tubing used to make this coil is approximately 0.28λ. At 7.2 MHz, the coil conductor becomes approximately 0.53λ. Provision for current that is not constant could improve the results to a signficant degree, and this refinement represents a second activity reserved for future work.

The collection of MATLAB code(s) required to make new individualized proximity loss calculations is not yet in a user-friendly form. Work toward having a final software product that can be made available in the public domain is continuing.

A practical finding of this work is that compact multiturn loop antennas similar to one studied in detail here may, indeed, be effective as portable/mobile antennas for HF communications if fed with coaxial line of appreciable length (at least 15 meters) without the ferrite choke assembly employed in this study to suppress currents on the coax braid. In such unbalanced operation, it has been observed that the coil plus coax system becomes competitive with a half-wave dipole.

References

[1] *The ARRL Antenna Handbook, 19th Edition*, Newington, CT: The American Radio Relay League, 2000, Chapter 5 (especially pages 5-12 through 5-19).

[2] Hart, T., “Small, high-efficiency loop antennas,” *QST*, June 1986, pp. 33-36.

[3] Smith, G.S., “Radiation efficiency of electrically small multiturn loop antennas,” *IEEE Trans. Ant. and Prop*., Sept 1972, pp 656-657.

[4] Best, Stephen, Advances in Electrically Small Antennas, a short course at the *2004 IEEE International Symposium on Antennas and Propagation*, Monterey, CA, June 2004.

[5] Best, S.R.and Morrow, J.D.,"The effectiveness of space-filling fractal geometry in lowering resonant frequency," *Antennas and Wireless Propagation Letters* , Volume: 1 , Issue: 5 , 2002, p 112 - 115.

[6] Kraus, J.D. and Marhefka, R.J., *Antennas for All Applications, 3rd Edition*, New York: McGraw-Hill, 2002, pp. 217-220.

[7] Smith, G., “Proximity effect in systems of parallel conductors,” *J. Appl. Phys.*, vol. 43, no. 5, pp 2196-2203, May 1972.

[8] MATLAB is a registered trademark of The Mathworks, Natick, MA, web URL **http://www.mathworks.com/**.

[9] Web URL **http://mathworld.wolfram.com/EllipticIntegral.html.**

[10] Whipple, F.J.W., “Equal parallel cylindrical conductors in electrical problems,” *Proc. Roy. Soc.* (London) A 96, 465 (1920).

[11] Wheeler, H.A., “Fundamental limitations of small antennas,” *Proc. IRE*, vol. 35, pp 1479-1484, Dec. 1947.

[12] Whittaker, E.T. and Watson, G.N., A Course on Modern Analysis, 4th Edition, Cambridge, England: Cambridge University Press, 1952, Ch. 22.

[13] Abramowitz, M. and Stegun, I.A., *Handbook of Mathematical Functions*, New York: Dover Publications, 1 June 1965, Chapters 16 and 17.

[14] Bowman, F., *Introduction to Elliptic Functions with Applications*, New York: Dover Publications, 1981.

[15] Andrews, L.C., *Special Functions for Engineers and Applied Mathematicians*, New York: Macmillan Publishing, 1985, p. 110.

[16] EZNEC is a software product of Roy Lewallen, as described at http://www.eznec.com/.

[17] Vinoy, K.J., Jose, K.A., Varadan, V.K., and Varadan, V.V., "Resonant frequency of Hilbert curve fractal antennas," *Antennas and Propagation Society International Symposium*, 2001. IEEE , Volume: 3 , 8-13 July 2001, p 648 - 651.

[18] Xuan Chen, Safieddin Safavi Naeini, and Yaxin Liu, "A down-sized printed Hilbert antenna for UHF band," *Antennas and Propagation Society International Symposium*, 2003. IEEE , Volume: 2 , 22-27 June 2003, p 581 - 584.

[19] Best, S.R.and Morrow, J.D., "On the significance of current vector alignment in establishing the resonant frequency of small space-filling wire antennas," *Antennas and Wireless Propagation Letters* , vol. 2, no. 13, 2003, p 201 - 204.

[20] Vinoy, K.J., Abraham, J.K., and Varadan, V.K., "Fractal dimension and frequency response of fractal shaped antennas," *Antennas and Propagation Society International Symposium*, 2003. IEEE , Volume: 4 , 22-27 June 2003, p 222 - 225.